Original Article

Stress tensors and quantification of fracture patterns to analyze connectivity and potential fluid flow in a mesa landform of the Northern Andes

GARCÍA-ARIAS Sergio[1]* (iD) https://orcid.org/0000-0002-9644-8568; ✉ e-mail: sergio.garcia.910815@gmail.com

VELANDIA Francisco[1] (iD) https://orcid.org/0000-0001-6263-0903; e-mail: favelanp@uis.edu.co

ALVAREZ Angélica[1] (iD) https://orcid.org/0000-0001-9196-3264; e-mail: aalvarna@correo.uis.edu.co

SANABRIA-GÓMEZ José D[2] (iD) https://orcid.org/0000-0002-4217-3212; e-mail: jsanabri@uis.edu.co

TARAZONA Yessenia[1] (iD) https://orcid.org/0000-0003-2923-6159; e-mail: yessetaraliz@gmail.com

VARGAS María Camila[1] (iD) https://orcid.org/0000-0002-0732-3203; e-mail: mariac_0603@hotmail.com

* Corresponding author

1 Escuela de Geología, Universidad Industrial de Santander, Cra. 27 Calle 9, Bucaramanga, Colombia

2 Escuela de Física, Universidad Industrial de Santander, Cra. 27 Calle 9, Bucaramanga, Colombia

Citation: García-Arias S, Velandia F, Alvarez A, et al. (2024) Stress tensors and quantification of fracture patterns to analyze connectivity and potential fluid flow in a mesa landform of the Northern Andes. Journal of Mountain Science 21(1). https://doi.org/10.1007/s11629-023-8338-5

Abstract: This work applies stress tensors inversions and quantification of fracture patterns along the Mesa de Los Santos, in the Eastern Cordillera of Colombia, to better understand the potential fluid flow. It thus contributes to the conceptual hydrogeological model. The area was subdivided into three blocks, separated by the NW Potreros and the Los Santos faults, having minor inner faults of different orientations. This separation facilitates the analysis of the fractures measured in the field, which in general show high dip angles and a conjugate geometry in the northern block, tension fractures (Mode I) in the central block, and a random distribution in the southwestern block. Win-Tensor treatment of slickensides yielded a maximum horizontal stress (SHmax) of 111º, which coincides with the WNW-ESE tensor observed from the conjugate and tension joints. We then used FracPaQ to generate interpolation maps of fracture intensity and density. The maps show the highest values in the central block and the lowest in the northern block, where the precipitation is higher, causing intensive rock weathering and homogenization of the fracture planes. Although the highest values of connectivity by line are found to the south of the mesa, we suggest the possibility of greater flow from the recharge zone (NE) along bedding planes and open NW-SE fractures.

Keywords: Mesa de Los Santos; Colombia; Win-Tensor; FracPaQ; Strike-slip faults; Fractured aquifers

1 Introduction

The flow paths in fractured rock aquifers can change from meters to kilometers in scale, due to fracture distributions (which are sometimes not uniform) and connectivity and variable hydraulic properties (Shapiro et al. 2007). The combination of different techniques in structural geology allows the characterization of fractures, which indicate certain rock properties. This, in turn, affects fluid flow and therefore can be used to determine secondary porosity.

Many numerical modeling studies cover various issues related to fracture connectivity and permeability, including site characterization, model validation, scale dependence and the effects of fracture density, length, and aperture distributions (Mortimer et al. 2011).

The hydraulic properties of rocks are controlled by fractures as they provide permeable conduits for fluids. However, not all fractures or faults contribute to fluid flow (Long et al. 1991; Finkbeiner et al. 1997). Groundwater flow within fractured rock aquifers is primarily influenced by fracture density, length, geometry, connectivity, infill, weathering, and the effects of the present-day in situ stress field (National Research Council 1996). In crystalline and sedimentary rocks, fractures and faults (potentially active under the current stress field) are the most permeable and critical features controlling fluid migration and diagenetic processes (Isaacs 1984; Barton et al. 1995; Finkbeiner et al. 1997). In the presence of different horizontal stresses, faults, and fractures with strikes parallel to the maximum horizontal compressive stress (SHmax) tend to open, while those with strikes perpendicular to the (SHmax) tend to close (Ferrill et al. 1999). The maximum permeability for the fluid flow occurs along fractures that are favorably aligned within the in-situ stress field. Preferential flow takes place along fractures oriented orthogonal to the minimum principal stress direction, due to low normal stress, or inclined ~30° to the maximum principal stress direction, resulting from dilation (Barton et al. 1995; Mortimer et al. 2011). For example, research conducted at Yucca Mountain in Nevada, USA, concluded that faults that are favorably oriented for slip in the current stress field play a significant role in controlling local groundwater flow (Ferrill et al. 1999). These faults also serve as pathways for upward flow in the saturated zone, facilitated by increased small-scale fracturing and faulting in the vicinity of faults on the verge of shear failure (Fridrich et al. 1994; Barton et al. 1995; Bredehoeft 1997; Finkbeiner et al. 1997). The estimated anisotropic transmissivity has a maximum principal direction controlled by faults and fractures within the present-day in situ stress field (Ferrill et al. 1999). Other studies conducted in the Santa Maria Basin (California, USA), as documented by Finkbeiner et al. (1997) indicate that the occurrence of earthquakes provides evidence of active shear deformation and faulting processes; these planar features are potentially active reverse or strike-slip faults. The permeability of the formation is enhanced at depth intervals with brittle lithology and critically stressed fracture and bedding planes that strike perpendicular or oblique to the maximum horizontal stress - SHmax (Finkbeiner et al. 1997).

The research area is described as a mesa landform, although the strata exhibit more than horizontal dips. The Mesa de Los Santos serves as a regional development hub, particularly for agriculture and tourism. However, water scarcity poses a limitation, leading to increased exploitation of groundwater resources. The aquifer system in the Mesa de Los Santos is considered a double porosity aquifer, but at a local scale it functions as a fractured aquifer (Pinto et al. 2007), where the recharge is mainly dependent on precipitation (Becerra and Parra 2016). It is essential to develop a conceptual hydrogeological model for an effective water resource management, and our research findings contribute to this endeavor.

The mesas area is located north of the axial zone of the Eastern Cordillera of Colombia, in the Northern Andes (Fig. 1). Within this regional landscape, the Mesa de Los Santos is the most outstanding feature (Julivert 1958), consisting of a sequence of continental to marine sedimentary rocks (Royero and Clavijo 2001) bounded by the Bucaramanga Fault to the east, the Chicamocha river to the south, and the Sogamoso river to the west (Fig. 1). The current tectonic frame is related with recent fault activity (Paris et al. 2000) and permanent intermediate seismicity from the Bucaramanga Seismic Nest (Taboada et al. 2000).

Previous geological studies conducted by Pinto et al. (2007) contributed valuable information to support a hydrogeological model for the Mesa de Los Santos. The studies specifically focused on structural geology include the mapping of the main geological faults within the mesa (Vargas 2008), the analysis of stress tensors and their kinematic interpretation (Velandia et al., 2007), joint analysis (Contreras 2008), and an approximation to hydrogeology (Díaz et al. 2009; Velandia 2010). More detailed studies involving fracture measurement and geological fault mapping (Tarazona-Lizcano et al. 2021), along with the present work, provide new data and advancements for structural interpretation, including the study of fracture patterns using updated techniques. Given the continuous seismic activity in the area due to the Bucaramanga Seismic Nest, as well as the potential activity of faults with neotectonic features (Paris et al. 2000; Velandia and Bermúdez 2018; Velandia et al. 2020) it is crucial to understand the behavior of

fractures, their connectivity, and their potential influence on the hydrogeological system. In the same sense, the precipitation data analysis is a crucial factor for the comprehension of the groundwater recharge (Fig. 2).

Firstly, we employ a kinematic interpretation of geological faults based on local stress tensors, obtained from rock outcrop data, particularly through the measurement of striated planes. Subsequently, fracture patterns are analyzed using quantitative techniques through photographs of representative outcrops to identify attributes such as intensity, density, connectivity, and permeability, contributing to the characterization of potential flow corridors. To achieve these goals, we used the Win-Tensor program (Delvaux 2001; Delvaux and Sperner 2003) and a methodology supported by FracPaQ, a statistical processing program (Healy et al. 2017; Healy and Rizzo 2019), as well as Kriging methods to obtain interpolation maps of the fracture analysis. It is important to note that the traces exposed on the rock surface considered in this study are rarely uniform, as fractures often exhibit varying degrees of order or relationships, which can influence the mechanical (e.g., strength, anisotropy) and transport properties of the rock (e.g., fluids, heat) (Healy et al. 2017).

and Caribbean plates, along with the Chocó-Panamá Block defines the current tectonic configuration of the Northern Andes, including the Eastern Cordillera of Colombia (Kellogg et al. 1995; Taboada et al. 2000), where the "mesas and cuestas zone" is located. Cortical seismicity (<40 km) is shown in Fig. 1 (from the National Seismological Network of Colombia) to infer the brittle deformation of the cordillera and its relationship with the geological faults. Focal

Fig. 1 A. Map of northern Colombia with the location of the Mesa de Los Santos on the western flank of the Eastern Cordillera. B. The Mesa de Los Santos constitutes a lower elevation zone defined to the south by the Chicamocha river and structurally controlled to the east by the Bucaramanga Fault and to the west by the Suarez Fault. Focal mechanisms from Londoño et al. (2019) and Machuca, et al. (2021). Cortical seismicity (<40 km) and Bucaramanga Seismic Nest (140 to 160 km) data sourced from the National Seismological Network of Colombia.

2 Geological Setting

The interaction of the Nazca, South American,

Fig. 2 A. Geographical distribution of the 101 IDEAM stations across the department of Santander, Colombia. B. The rainfall data are interpolated using the Kriging method to obtain an average annual rainfall map from 2000 to 2020.

mechanisms define a predominance of strike-slip regimes with a WNW-ESE current stress tensor, although none of these are located around the Mesa de Los Santos. The maximum horizontal stres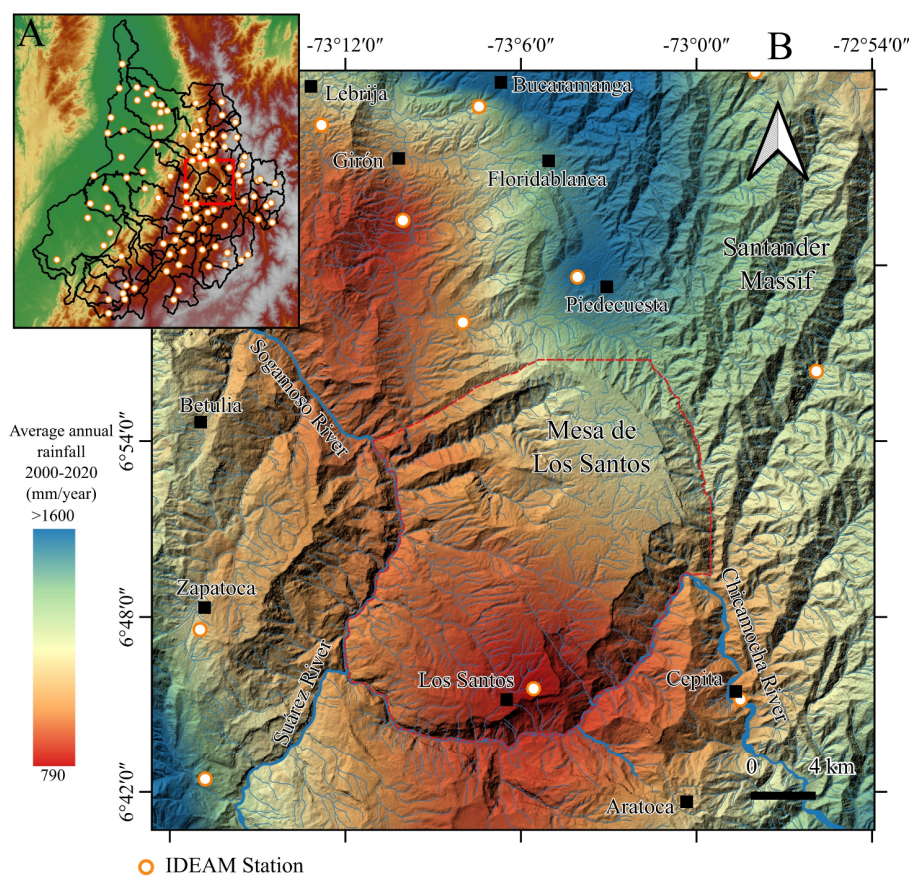s (SHmax) obtained from focal mechanisms for the Santander Massif and its surroundings, perfectly explains the sinistral kinematics of the Bucaramanga and sub-parallel faults (Londoño et al. 2019; García-Delgado et al. 2022) and coincides with the general and current orientation of the SHmax calculated from slickensides by Velandia et al. (2020).

The mesa is also renowned for being the epicenter of earthquakes originating from the Bucaramanga Seismic Nest (van der Hilst and Mann 1994; Malavé and Suárez 1995; Taboada et al. 2000; Zarifi and Havskov 2003). The seismicity of the nest is concentrated around a depth of 150 km, being one of the most active in the world considering the number of earthquakes with Magnitude > 4 (Prieto et al. 2012). Here we only show Magnitude > 5 from the nest (Fig. 1) to strengthen the notion that both, cortical and

intermediate earthquakes potentially impact water levels and fluid dynamics in the region, although this aspect lies beyond the scope of this study.

The Mesa de Los Santos basement consists of Paleozoic low-medium grade metamorphic rocks of the Silgará Fm. (Ward et al. 1977), differentiated from the Chicamocha Schist by Mantilla-Figueroa et al. (2016), and Early Jurassic igneous intrusive bodies associated with the Pescadero Granite (Ward et al. 1977). The unconformable Jurassic continental "red beds", named in the region as the Jordán Fm. (Cediel 1968) having some component of felsic volcanic rocks (Alarcón et al. 2020). A tectonic pulse at the end of the Jurassic and beginning of the Cretaceous is evidenced by Los Santos Fm. (mainly quartz sandstones in the upper part) and its angular unconformity over the Jordán Fm. (Alarcón and Rodríguez 2019; Laverde 2023). Marine Cretaceous rocks are recognized as the Rosa Blanca (limestones and mudstones), Paja (shales) and Tablazo (limestones and mudstones) formations (Julivert et al. 1964; Laverde 1985; Pinto et al. 2007; Díaz et al. 2009) (Fig. 3).

The structural framework of the Mesa de Los Santos is defined by the Bucaramanga Fault to the east, a regional sinistral transpressional structure (Velandia et al. 2020), which separates the mesa from the Santander Massif, and shows geomorphological features of neotectonic activity (Paris et al. 2000; Velandia and Bermúdez 2018; García-Delgado et al. 2020). To the west, the landscape is dominated by the Suárez Fault, a reverse structure along the Suárez River valley that shows evidence of recent activity from north to south, with lateral propagation of folds in its hanging block, at the Yariguíes Range (Machuca et al. 2021). Los Montes Fault is a minor structure (dextral transtensional) that divides the Mesa de Los Santos
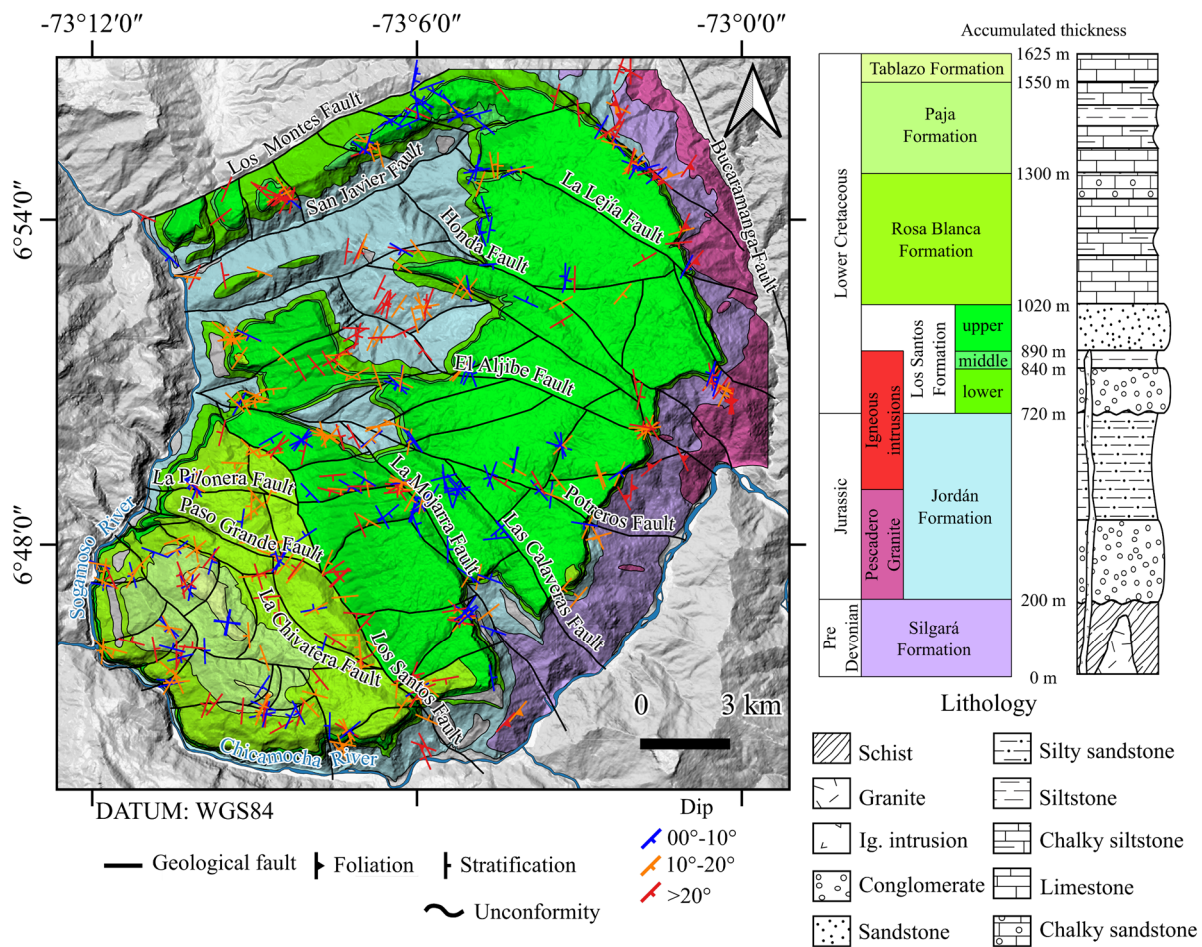
Fig. 3 Geologic map and stratigraphic sequence of the outcropping units in the Mesa de Los Santos. Modified from Pinto et al. (2007).

from another contiguous feature to the north, the Mesa de Ruitoque (Fig. 1).

The Mesa de Los Santos shows three main structural trends with distinctive kinematics: (i) an NW orientation, corresponding to the main and most continuous faults, (ii) an NE trend, with faults limited between the previous ones, and (iii) an EW trend, with minor faults observed especially in the southern part of the mesa (Pinto et al. 2007; Contreras 2008; Vargas 2008). Among the NW structures, the Los Santos Fault is the most conspicuous feature (Fig. 2), previously considered of minor extension, but recently Velandia et al. (2020) described it as a regional structure, with a subparallel trend and similar kinematics to the Bucaramanga Fault, connected to the Lebrija fault to the north, and extending farther south.

The fractures in the area were studied using a hydrogeological approach by Contreras (2008) and Díaz et al. (2009). Taking the distribution of open and closed joints, their density, and dip ranges, they

proposed water flow along the bedding, and sectors where aquifers are configured by interconnected fractures that allow recharge. The shallow depth of the wells located in the area shows that the upper member of the Los Santos Formation is the main aquifer and the most exploited in the area (Contreras 2008).

3 Methods

The geological map of Pinto et al. (2007) was used as the baseline for the geological faults of the Mesa de Los Santos (Fig. 3). This work refined the existing traces, and complemented and detailed the mapping of associated synthetic and antithetic fault traces along the shear zones to determine their kinematics by using shaded relief maps extracted from DEMs with 30 and 12.5 m resolution (NASA 2020), and satellite images from Planet Team (2018). The stress tensors and fracture analysis are based on field measurements of

striated fault planes and joints. Additionally, a quantitative analysis of fracture patterns was performed using photographs of representative outcrops from the study area.

3.1 Stress tensor calculation and kinematic analysis

Kinematic analysis provides insight on how a rock body responds to deformation, in terms of how it changes location, orientation, shape, and size (Marrett and Peacock 1999; Davis et al. 2011). At the outcrop scale, this is achieved by measuring displacement indicators such as fault striations, Riedel-type planes, and neo-mineralized steps, among others (Huang and Angelier 1989). Combining as many of these "dominant hierarchy" kinematic criteria as possible yield the best possible analysis (Petit 1987; Doblas 1998; Fossen 2010).

We investigated the kinematics by measuring slickensides (dip direction and angle of planes, and pitch and pitch-direction of lines), and defining sense of movement from Riedel and anti-Riedel surfaces and other indicators (Petit 1987; Doblas 1998), as well as a parameter for the degree of reliability. Following Angelier (1994) we used four planes preferably with different orientations for the calculations of the stress tensor. Data processing was performed in Win-Tensor 5.9.2 software (Delvaux 2001), which allows user-controlled data inversion to avoid program bias due to overestimation of low to medium-quality data.

In the applied methodology following Delvaux and Sperner (2003) and Velandia (2017) the processing starts with the Enhanced Straight Dihedron method filtering the data until reaching counting values of 0% and 100% for σ_1 and σ_3 respectively, and a counting deviation < 30. This allows filtering planes on the Mohr circle, of the neoformed and reactivated fractures. The filtered data were processed with the Rotational Optimization method, which seeks to minimize the average mismatch angle between the modeled and observed slip directions. This helps to obtain the best "Tensor Quality Rank" criteria to evaluate the amount of data, its confidence level and the percentage of used data (Delvaux and Sperner 2003). It also helps to maximize the "World Stress Map Quality Rank", which is a global standard of the quality of SHmax orientation measurements (Zoback 1992). Each obtained tensor solution can be supervised with the histogram of misfit function F5, with values tending to zero. The stress ratio R is represented by $(\sigma_2 - \sigma_3)/(\sigma_1 - \sigma_3)$, but the stress regime can be more practically quantified by the indicator R' (Table 1), so that R'= R extension, R'= 2-R transcurrence, and R'= 2+R compression (Delvaux et al. 1997).

Table 1 Stress regime from the R' index. From Delvaux et al. (1997).

Stress index R'	Vertical stress (σ_v)	Stress Regime
0.00-0.25	σ_1	Radial extensive
0.25-0.75	σ_1	Pure extensive
0.75-1.25	σ_1 o σ_2	Transtensive
1.25-1.75	σ_2	Pure Strike-Slip
1.75-2.25	σ_2 o σ_3	Transpressive
2.25-2.75	σ_3	Pure compressive
2.75-3.00	σ_3	Radial compressive

To determine the mechanical coherence of each stress tensor, the resulting Mohr circle was checked by verifying whether the data were associated with newly formed (neoformed) or reactivated fractures (Fossen, 2010). From the orientation of the SHmax or stress tensor, it is possible to determine the kinematics of the geological faults by decomposing the tensor and obtaining the normal and shear vectors. In examining the correlation between SHmax and the existing stress regime, we conduct a comparative analysis juxtaposing our findings with previously computed focal mechanisms and stress tensor trajectories from prior regional studies encompassing the area (Cortés and Angelier 2005; Londoño et al. 2019; Velandia et al. 2020; Machuca et al. 2021; García-Delgado et al. 2022).

3.2 Fracture patterns quantification

Characterizing the degree of fracturing in two dimensions (2D) allows the finding of statistical distributions and relationships between its geometric parameters (Mauldon et al. 2001; Rohrbaugh et al. 2002; Zeeb et al. 2013). This can be done using FracPaQ (Healy et al. 2017), which is an open-source tool written in MATLAB™ (The MathWorks Inc. 2022). This software generates Rose diagrams of lineaments and estimates their intensity, density, average lengths, connectivity (by considering the ternary connectivity plot proposed by Manzocchi (2002), fracture matrix (Oda 1982; Oda et al. 1987), and permeability ellipse (Suzuki et al. 1998).

For the processing in FracPaQ 2.6, lineaments were manually digitized from the photographic log and recorded parallel to the outcrop (Fig. 4). The reference

bearing and scale were recorded for later calibration (north and scale) in the software. By default, the north is set on the positive Y axis, while for the scale the pixel is the predefined unit. FracPaQ uses the circular window sampling method (Mauldon et al. 2001) and takes the specified number of scan circles as the minimum number of those used along the shortest side of the area (Healy et al. 2017).

In the Maps section of the software, the estimated intensity (P21) and estimated density (P20) analysis were selected, considering 12 circular windows. For the circular windows it is necessary to consider the number of intersections between the fractures and the outer circumference to determine the fracturing intensity:

$$I = \frac{n}{4r},\qquad(1)$$

where n is the number of intersections between the circumference of the sample window and the fracture traces, and r is the radius of the circumference used by Mauldon et al. (2001).

Fracture density refers to the number of fractures per unit area and is expressed as

$$\rho = \frac{m}{2\pi r^2},\qquad(2)$$

where m is the number of fracture initiations and terminations within the sample window, and r is the radius of the circumference used by Mauldon et al. (2001).

The ternary connectivity graph is obtained in the Fluid Flow section of the software. Connections by lines (CL) consider nodes I (isolated ends of traces), Y (branch points, splays, or abutments), and X (transverse intersections). According to Sanderson and Nixon (2015), CL is expressed as
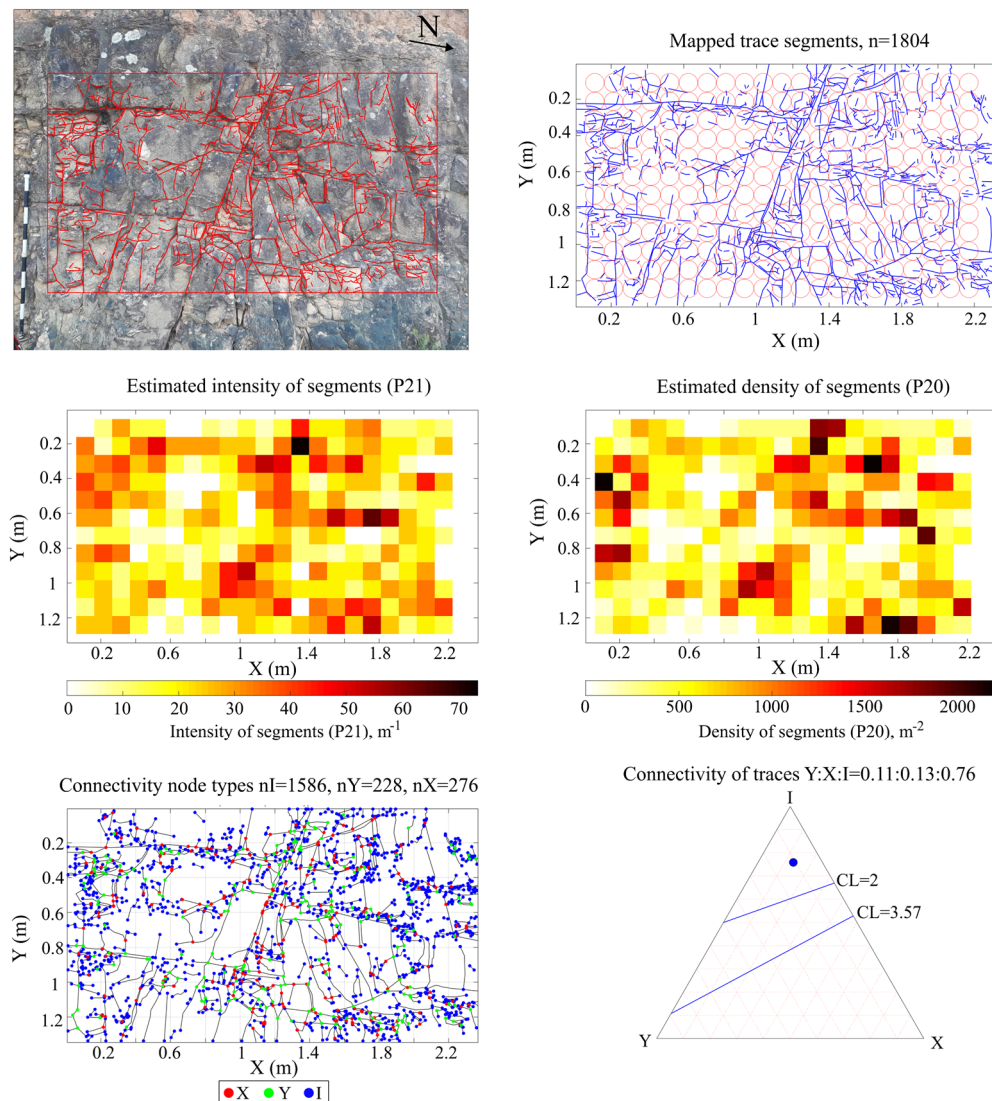

Fig. 4 Sample outcomes derived from the FracPaQ tool showing photographic records after lineament tracing, north, and scale correction.

$$CL = 4 \frac{N_Y + N_X}{N_I + N_Y}. \tag{3}$$

The strike and dip of the fracture planes measured in the field are represented with Rose diagrams using GeoRose 0.5.1 software (Yong Technology Inc. 2014) and compared with the results obtained from FracPaQ. We also used Stereonet 11 software (Allmendinger et al. 2011; Cardozo and Allmendinger 2013) to plot poles of fracture-associated and striated planes.

4 Results

Despite the relative geomorphological and structural homogeneity of the Mesa de Los Santos, the geological mapping and fracture data can distinguish at least three zones, or blocks, with different geological fault behavior (orientations and kinematics). The northern block is characterized by geological faults with two distinct orientations (Fig. 5): the NW-SE trending Los Montes Fault marked the northern boundary of the mesa; and the NE-SW trending Potreros Fault is defined as the southern boundary of the block. The central block is bounded to the SW by the Los Santos Fault and shows inner parallel structures that control the extension of minor transverse faults. The southwestern block is defined by a more complex system of faults crossings W-E and N-S, and other subparallel trends to the Los Santos Fault.
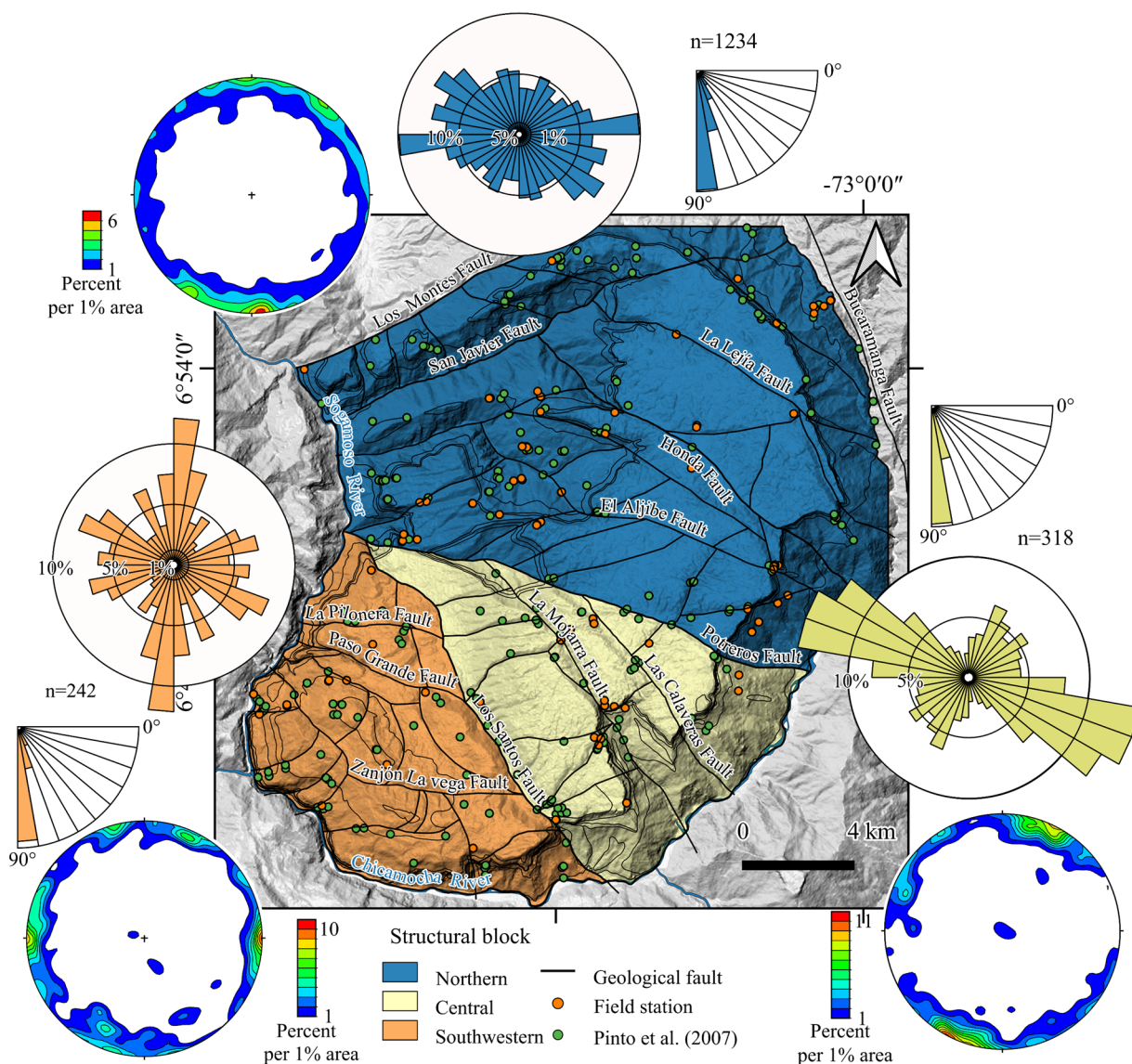

Fig. 5 Rose diagrams and pole density (generated in GeoRose and Stereonet software respectively) of the fracture planes measured in the field (orange dots). Pinto et al. (2007) station locations (green dots) are included for the three differentiated structural blocks.

This fault also divides the sandstones of the Los Santos Formation to the north from the limestones and mudstones of the Rosa Blanca and Paja formations to the south (Fig. 3). The faults' kinematics and structural style in these three blocks of the mesa will be explained later, however, this division is a simplification of those proposed by Pinto et al. (2007) for the entire mesa and by Tarazona-Lizcano et al. (2021) for the southern zone.

Here, we show the results of the analysis of 72 field stations, which focus on the orientation of joint planes, calculation of stress tensors, and quantification of fracture patterns. Planes associated with stratification or foliation were identified in 40 of the 72 stations, where 87% have a dip of less than 30°. To complement the orientation of the fracture planes, we also used the INGEOMINAS-UIS project database (Pinto et al. 2007).

4.1 Joint orientation

We used a total of 1794 fracture planes for the joint orientation analysis at the Mesa de Los Santos: 1234 for the northern block, 318 planes in the central block, and 242 in the southwestern block. More than 75% of the fracture planes have a dip greater than 70°.

Inside the northern block there are two main structural trends: the NE-trending San Javier and Los Montes faults, and the NW-trending Potreros, El Aljibe, Honda, and La Lejía faults (Fig. 5). These two trends show conjugate structures, a relationship that is

verified by the statistical orientation of the Rose diagram (Fig. 5, in blue), with main fracture planes of NW-SE (between 120°-140°) and W-E trends (between 80°-90°), where a difference of up to 60° is noted, considering the extreme values. Inside the central block, the La Mojarra and Las Calaveras faults are very parallel to the Los Santos Fault (NW-SE), but the fracture planes show a trend very similar to the strike of the Potreros Fault (Fig. 5, in yellow). The fracture planes of the southwestern block exhibit three preferential directions, which are parallel to the geological faults of the sector (Fig. 5). For this block the N-S trend is the main one in the Rose diagrams, but the 70°-80° and 100°-130° trends also stand out, and this latter trend coincides with the strike of the La Pilonera and Paso Grande faults (approx. 110°) (Fig. 5, in orange).

4.2 Stress tensors and kinematics analysis

The stress tensors can be found by processing planes with fault striations. By combining this information with the stress field and structure of the Mesa de Los Santos, it is possible to gain a sense of their kinematics. By extension, this also defines potential groundwater flow corridors. A total of 126 striated planes were identified in 19 of the 72 stations; six of these stations exhibit a reliable calculated local tensor (Table 2), with enough striated planes with different orientations, all located in the quartz

Table 2 Results from the processing of the sets of striated planes associated with faulting, relating the location of the generated tensors, the number of striated planes (n) associated with the tensor, the number of measured (nt) structural data, the orientation of the principal stresses (σ_1:S1, σ_2:S2, σ_3:S3), the orientation of the maximum (SHmax) and minimum horizontal stress (SHmin), the R and R' ratios, the statistical parameters: α (average error angle between the observed and modeled slip direction), F5 (mean value of the optimization function), the World Stress Map Quality Rank (QRw), the quality Tensor Quality Rank (QRt), and the stress regime (Table 1) deduced by Win-Tensor. Tensors S50, S62, S48, S11, S16, and S04 are within the stratigraphy of Los Santos Formation.

Tensor	S50	S62	S48	S11	S16	S04	All data
Long.	-73.061	-73.029	-73.077	-73.149	-73.142	-73.182	
Lat.	6.911	6.836	6.759	6.846	6.857	6.900	
n	6	23	19	18	5	7	74
nt	6	30	24	23	5	13	126
S1	18/158	01/285	06/286	12/115	02/129	15/315	09/290
S2	69/307	82/187	77/170	70/350	88/307	72/103	78/156
S3	10/065	08/015	12/017	16/208	00/039	09/223	09/022
R	0.76	0.06	0.21	0.34	0.60	0.40	0.50
R'	1.24	1.94	1.79	1.66	1.50	1.60	1.50
SHmax	156	105	106	116	129	134	111
SHmin	66	15	16	26	39	44	21
α	3.8	7.1	6.0	4.4	3.1	7.7	9.0
F5	1.8	2.1	1.7	1.2	1.9	3.0	3.6
QRw	D	B	B	C	E	D	B
QRt	D	C	C	E	E	D	B
Stress Regime	Transtensional	Transpressional	Transpressional	Pure strike-slip	Pure strike-slip	Pure strike-slip	Pure strike-slip

sandstones of the Los Santos Formation. During the data processing stage, the mechanical coherence of the tensors was controlled by Mohr's circle analysis, considering only the data corresponding to newly formed or reactivated faults. The tensors are considered to indicate the current stress field, as most of the measured planes (Table 2) and the six tensors are comparable in terms of the SHmax orientation and stress regime. Furthermore, they could represent a solution of the regional tensor, following the

methodology and regional considerations of Sassi and Faure (1996), Tripathy and Saha (2013), and Velandia and Bermúdez (2018).

In general, the six stress tensors show a transcurrent regime (pure strike-slip or transpression) and an NW-SE orientation of the SHmax, almost parallel to most of the major faults of the Mesa de Los Santos. The SHmax varies from 156° at station S50 to 105° at S62 (Table 2), although most show an WNW-ESE trend (Fig. 6), with stress axes that are
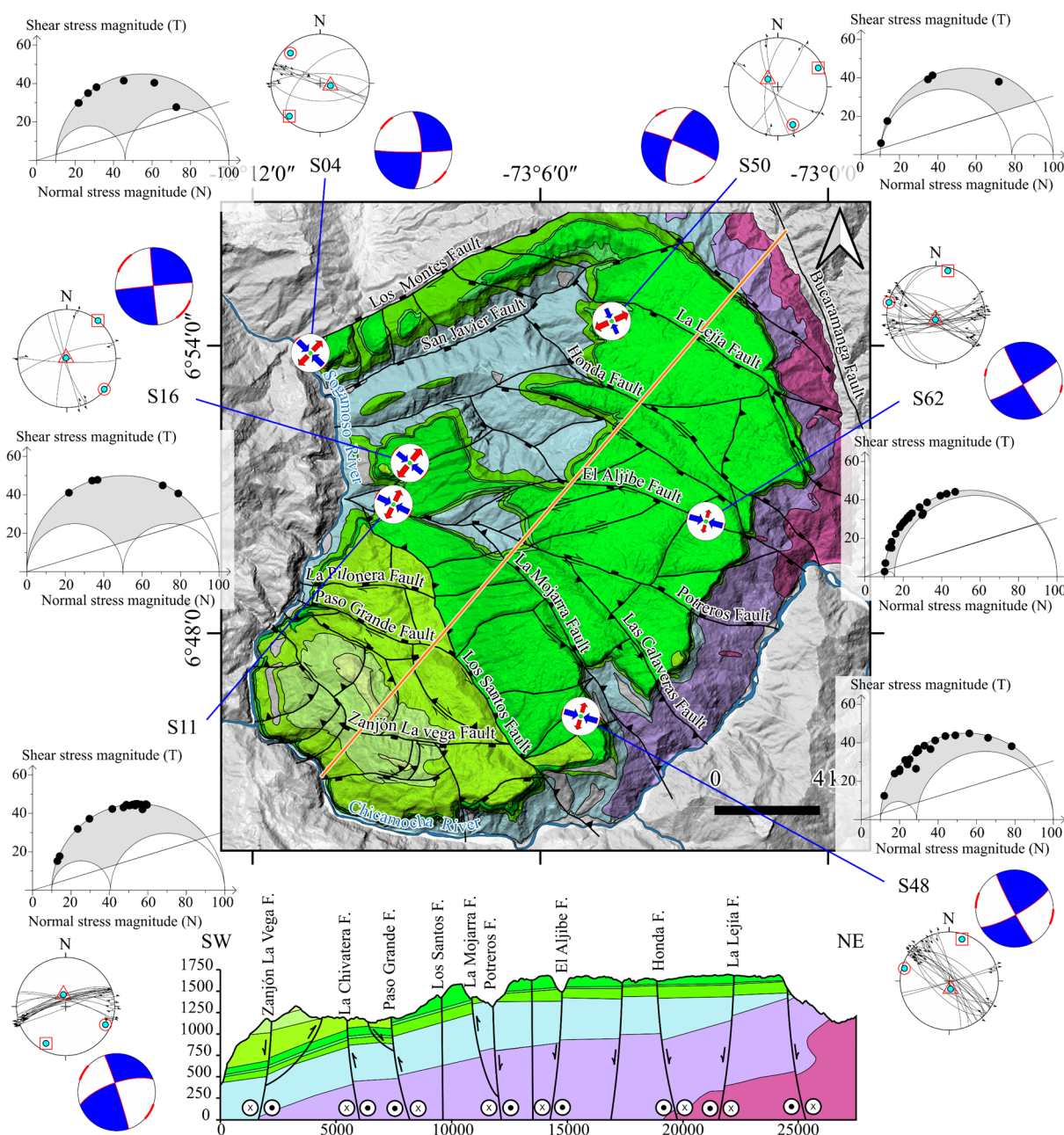

Fig. 6 Location of the six local tensors obtained in the Mesa de Los Santos. The general tensor obtained using all the striated data averages a σ1 orientation of 290° for the Mesa de Los Santos. The schematic geologic cross-section considers the new structural model and the geological units from Pinto et al. (2007).

geometrically ideally oriented, with two horizontal and one vertical. The pure strike-slip stress regime is confirmed with the vertical orientation of σ₂, as most of the structural planes show high dip and low pitch values for the fault striations. This is also illustrated by the solution of the stress tensors, represented as beach balls (Fig. 6).

Given the relative geological homogeneity of the area, especially of the northern and central blocks (where the Los Santos Formation outcrops), we decided to obtain a general stress tensor for the area, considering all the data measured in the 19 field stations (Table 2, Fig. 7). A graphical way to summarize

the tectonic strike-slip regime of the area is the Frohlich Ternary Diagram (Fig. 7B). This plots the data used to obtain the tensor, according to whether they are predominantly strike-slip, compressional, or extensional regimes, or some combination thereof (Frohlich 1992, 2001). In addition, the result of the general tensor yielded a SHmax of 111° and an R' of 1.50 confirms the pure strike-slip stress regime.

Based on the orientation of this stress tensor, geologic relationships, and topographic differences, it is possible to define the kinematics of the geologic faults (Fig. 6). In the northern block, the main faults are subparallel to the SHmax, so they have a dip
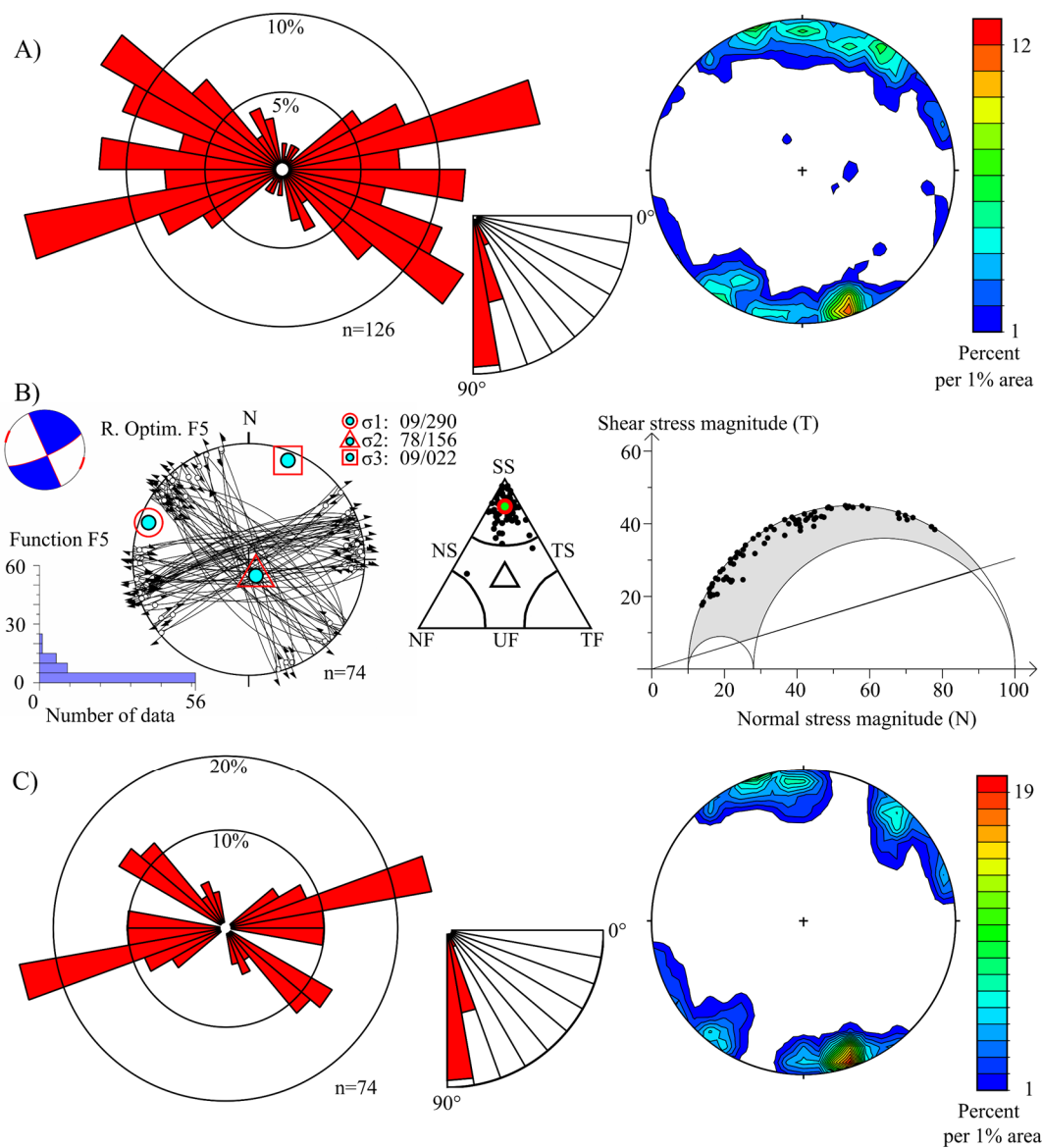

Fig. 7 General tensor. A) Rose diagrams and pole density diagrams of the planes measured in the Mesa de Los Santos. B) Stress tensor including the stereographic projection of the striated planes, Frohlich diagram, and Mohr circle. C) Rose diagrams and pole density diagrams of the fault planes processed for the stress tensor.

component similar to normal faults (Fig. 6). Due to some small differences in orientation, their strike component can be sinistral (La Lejía and Honda faults) or dextral (El Aljibe and Potreros faults). In the central block, Los Santos, La Mojarra, and Las Calaveras faults are parallel to each other and have a more oblique-orthogonal geometric relationship with the SHmax, therefore they are transpressional (sinistral and inverse). Structurally, the southwestern block is more complex due to the variety of outcropping geological units and the different orientations of the geological faults, which, compared to the SHmax, imply different kinematics: NW-SE faults as transpressional, W-E faults as transtensional and NE-SW faults as reverse (Fig. 6).

4.3 Intensity and density of discontinuity planes

In terms of density and intensity of the discontinuity planes, we analyzed the data with FracPaQ and then we used the Kriging method to interpolate the outcrops results, obtaining a similar pattern among them (Fig. 8). The northern block (Table 3) exhibits low values for density (<287 lineaments m⁻²) and intensity (<16 lineaments m⁻¹), where the lowest is associated with the Los Santos Formation (upper member), especially towards the

northernmost sector of the Mesa de Los Santos. In contrast, the highest values of density (>616 lineaments m⁻²) and intensity (>20 lineaments m⁻¹) are in the central block (Table 4), on poorly weathered quartz sandstones of the same upper member of the Los Santos Formation, affected by the Las Calaveras, La Mojarra and Los Santos faults. The intermediate values of density (287-1065 lineaments m⁻²) and intensity (16-28 lineaments m⁻¹) are located in the southern part of the northern block, between El Aljibe and Potreros faults, and in the southwestern block (Table 5, Table 6).

4.4 Connectivity

The lineament connectivity associated with fracturing and layering in FracPaQ is represented using a ternary graph (Fig. 9), which considers the correlation of I nodes (isolated ends), Y nodes (branch points), and X nodes (intersections), where a greater number of Y and X nodes imply a location closer to the base of the ternary graph and greater connectivity. The results of each analyzed station are plotted according to the geological unit that outcrops there. The stations corresponding to the Pescadero Granite, the Silgará Fm., and the Jordan Fm. (Fig. 9) show low connectivity (located in the upper part of the ternary graph), along
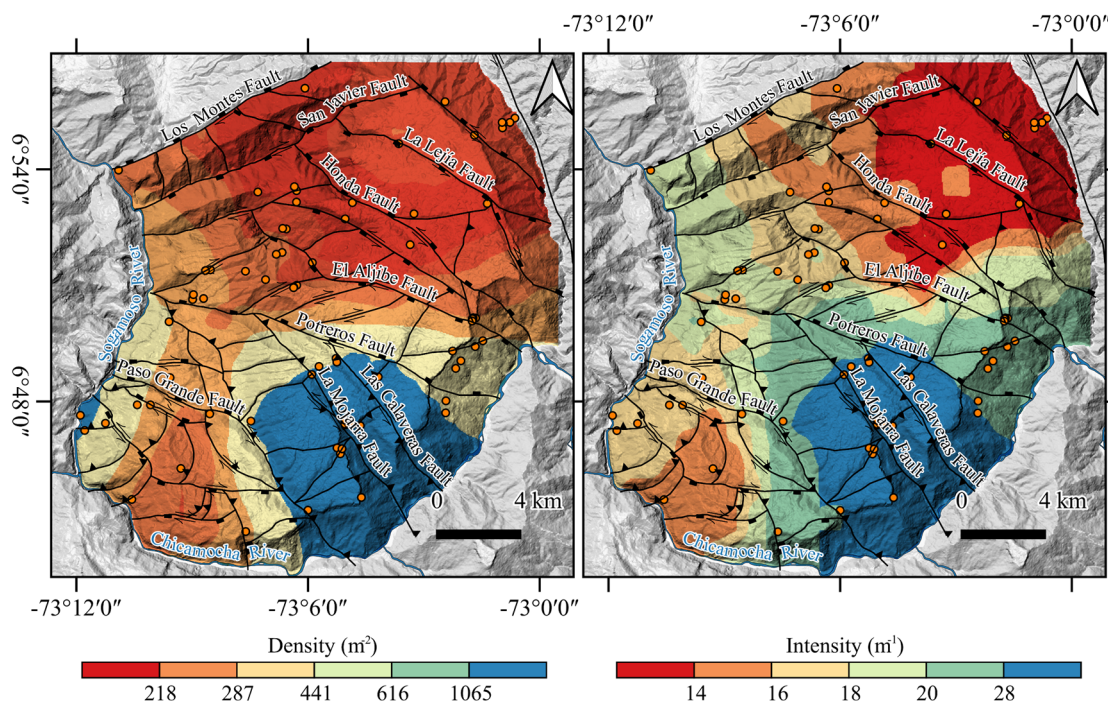

Fig. 8 Lineament intensity and density maps obtained by the Kriging interpolation method, considering the individual FracPaQ results of each of the field stations.

Table 3 Quantified results of fracture patterns in the northern block derived from stations with photographic records, processed using FracPaQ.

Station	Formation	Intensity m⁻¹	Density m⁻²	I nodes	X nodes	Y nodes	Cl
S12	Los Santos	21.66	1299.92	443	103	198	1.88
S13	Los Santos	5.60	21.88	1211	394	44	1.40
S17	Los Santos	21.28	213.11	295	103	42	1.72
S20	Jordán	7.93	29.27	284	79	12	1.23
S21	Los Santos	17.72	210.77	1917	644	130	1.51
S22	Jordán	41.25	1091.14	546	146	57	1.35
S23	Jordán	4.32	7.39	310	108	30	1.62
S24	Jordán	24.40	389.04	2574	680	226	1.29
S25	Jordán	16.70	300.42	314	42	31	0.85
S26	Los Santos	20.95	356.00	524	201	152	2.09
S27	Los Santos	9.57	58.16	2165	504	56	1.01
S28	Jordán	17.27	214.71	2353	535	192	1.14
S31	Los Santos	13.33	86.77	521	181	28	1.52
S32	Los Santos	11.53	79.52	2270	676	294	1.51
S35	Jordán	14.39	86.63	105	31	3	1.26
S43	Los Santos	13.65	254.34	347	33	36	0.72
S45	Los Santos	0.65	0.29	769	228	135	1.61
S50	Los Santos	29.80	618.58	735	156	55	1.07
S51	Los Santos	4.04	16.70	636	138	42	1.06
S52	Los Santos	7.10	47.49	369	97	17	1.18
S56	Los Santos	21.77	570.48	1586	276	228	1.11
S57	Silgará	17.19	146.56	95	20	9	1.12
S58	Silgará	42.57	2021.12	1917	258	25	0.58
S59	Los Santos	13.84	196.40	1150	271	52	1.07
S60	Los Santos	18.42	502.11	497	99	68	1.18
S61	Los Santos	9.42	81.24	489	59	29	0.68
S62	Los Santos	14.90	310.12	793	125	90	0.97
S63	Los Santos	11.55	212.68	3200	662	166	0.98
S64	Silgará	32.30	940.85	791	174	151	1.38
S65	Los Santos	1.37	1.06	1081	289	67	1.24
S66	Silgará	34.09	887.06	1775	349	58	0.89
S67	Los Santos	15.50	214.31	309	87	11	1.23
S68	Granito	17.42	164.19	154	53	19	1.66
S70	Granito	14.10	225.10	727	234	160	1.78
S72	Granito	20.87	294.77	129	52	9	1.77

Table 4 Quantified fracture pattern results for the central block obtained from stations with photographic records, analyzed using FracPaQ.

Station	Formation	Intensity m⁻¹	Density m⁻²	I nodes	X nodes	Y nodes	Cl
S19	Los Santos	27.46	1410.00	333	111	126	2.07
S33	Los Santos	18.36	353.00	293	115	100	2.19
S34	Los Santos	32.59	1240.00	626	168	262	1.94
S36	Los Santos	34.38	1220.00	356	143	122	2.22
S37	Los Santos	18.59	791.00	1126	239	691	2.05
S38	Los Santos	27.23	537.00	427	199	132	2.37
S39	Los Santos	18.18	510.00	366	153	227	2.56
S40	Los Santos	49.67	6060.00	1207	253	615	1.91
S41	Los Santos	20.71	842.00	752	189	419	2.08
S42	Los Santos	33.31	2130.00	2134	591	1389	2.25
S44	Los Santos	25.05	922.00	645	350	195	2.60
S46	Los Santos	43.63	2340.00	161	67	53	2.24
S47	Los Santos	52.95	2390.00	645	350	195	2.60
S48	Los Santos	38.19	2540.00	772	208	333	1.96
S49	Los Santos	29.15	1096.72	459	147	72	1.65
S54	Silgará	21.69	495.85	591	152	76	1.37
S55	Silgará	35.13	1299.66	1226	350	1	1.14

Table 5 Quantitative analysis of fracture patterns in the southwestern block derived from stations with photographic records and processed using FracPaQ.

Station	Formation	Intensity (m⁻¹)	Density (m⁻²)	I nodes	X nodes	Y nodes	Cl
S01	Los Santos	34.45	3550	268	78	184	2.32
S02	Rosa Blanca	15.85	262	536	207	136	2.04
S03	Rosa Blanca	13.66	632	1103	241	571	1.94
S05	Rosa Blanca	11.07	130	428	162	132	2.1
S07	Rosa Blanca	11.95	290	361	129	109	2.03
S08	Rosa Blanca	33.36	797.69	330	44	126	1.49
S09	Rosa Blanca	11.13	76.31	136	29	58	1.79
S10	Tablazo	4.95	34.1	56	27	33	2.7
S15	Rosa Blanca	6.84	0.58	512	204	72	1.89
S18	Rosa Blanca	4.73	14.64	42	7	18	1.67

Table 6 Local qualitative classification as proposed by Tarazona-Lizcano et al. (2021) assesses the intensity, density, and connectivity (Cl) of lineaments estimated by FracPaQ in the Mesa de Los Santos.

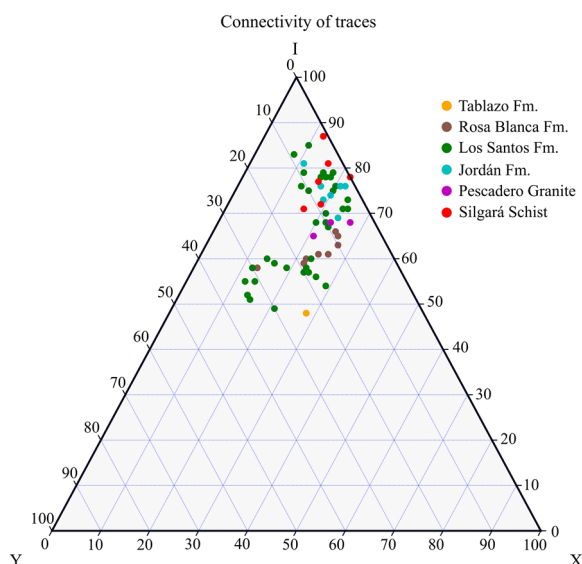| Qualitative classification	Intensity (m⁻¹)	Density (m⁻²)	Cl
High	>20	>616	>1.73
Medium	16-20	287-616	1.40-1.73
Low	<16	<287	<1.40

Fig. 9 Ternary diagram of connectivity of fracturing and layering lineaments estimated by FracPaQ, considering the correlation of I nodes (isolated ends), Y nodes (branch points), and X nodes (intersections). A higher count of Y and X nodes imply increased connectivity among the lineaments.

with some stations of the Los Santos Fm., although most outcrops of this unit are located with intermediate to high connectivity values. The stations associated with the Rosa Blanca Fm. show intermediate connectivity, while the only station of the Tablazo Fm. presents the highest connectivity value of the fractures and stratification planes of the Mesa de Los Santos.

The results of each station are interpolated with the Kriging method to obtain a lineament connectivity map (Fig. 10). The northern block of the Mesa de Los Santos has low connectivity by line (<1.40) up to the vicinity of El Aljibe Fault, where the stations plotting in the upper part of the ternary plot are located. Between El Aljibe and the Potreros faults (northern block) intermediate values (1.40-1.73) are estimated, while the highest values (>1.73) are found in the central and southwestern blocks, where the highest connectivity values correspond to outcrops of the Los Santos Formation (between the Potreros and Los Santos faults), and to a lesser extent, the stations located in the carbonate rocks of the Rosa Blanca and Tablazo formations.

4.5 Precipitation analysis

One of the direct applications of the previous results is to contribute to a conceptual hydrogeological model of the Mesa de Los Santos, in which finding a relationship between the geological conditions and ability of groundwater to flow from the recharge zone to sectors of possible discharge is key. For this reason, we collected precipitation data in the area at a multiannual level. For this reason, we used rainfall data over a time span of 2000 to 2020, taken from the *Instituto de Hidrología, Meteorología y Estudios Ambientales* (IDEAM 2022), collecting such data at 101 stations in the department of Santander (following Becerra and Parra 2016). The data are interpolated with the Kriging method to obtain a precipitation map of the Mesa de Los Santos (Fig. 2). Based on this information, it can be observed that the highest precipitation occurs in the north of the zone and decreases drastically in the central block, with extreme values right where the municipality of Los Santos is located.
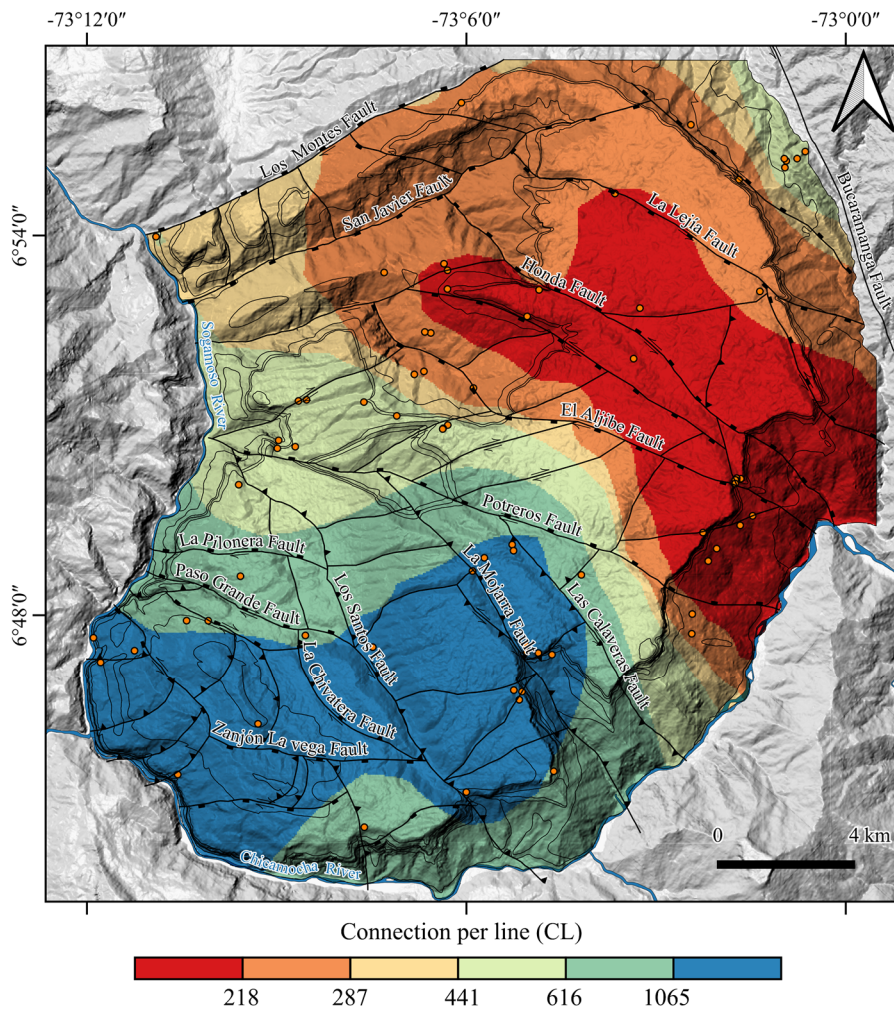
Connection per line (CL)

| 218 | 287 | 441 | 616 | 1065 |

Fig. 10 Lineaments connectivity map obtained through Kriging interpolation method considering the individual results of each of the field stations.

5 Interpretation and Discussion

Societal needs often require investigations into the formations properties that influence groundwater flow and chemical migration over increasingly larger spatial areas (Shapiro et al. 2007). Studying the connectivity of fracture networks involves a multidisciplinary perspective, incorporating methodologies such as hydrogeochemistry, geological mapping, borehole studies, and geophysics. This comprehensive approach is necessary due to the inherent heterogeneous nature of fractured rock aquifers (Mortimer et al. 2011). The diverse lithological settings and complexity of fracturing may lead to situations where one cannot immediately assume that the effective hydraulic conductivity is proportional to the measurement scale

(Shapiro et al. 2015). Here, we will discuss the kinematics of the geological faults of the Mesa de Los Santos, the quantification of fracture patterns, and the relationship of the structural model with the potential flow directions in a hydrogeological system.

5.1 Kinematic analysis of geological faults

The structural analysis considers regional aspects of faults, fracture orientation, and stress tensors to understand the kinematics of the geological faults in the Mesa de Los Santos. The main regional structure is the Bucaramanga Fault, which controls the course of the Chicamocha River from the SSE (Figs. 1 and 3). Its main trace has a pattern that includes minor Riedel-type faults, confirming its sinistral kinematics (Velandia and Bermúdez 2018). From the mouth of

the Manco River, the Chicamocha River abruptly changes its ENE to SW flow direction at a deflection bend (Fig. 1), where the traces of the Honda and El Aljibe faults converge, and may influence the structural control over fluvial dynamics. The Potreros Fault, the southern boundary of the northern block of the Mesa de Los Santos (Fig. 5), is an anti-Riedel trace (R') due to its convergence angle (approx. 60°), with respect to the main trace of the Bucaramanga Fault. This agrees with the dextral kinematics for this conjugate fault, as well as the parallel El Aljibe Fault in the Mesa de Los Santos. Meanwhile, the faults that exhibit smaller convergence angles to the Bucaramanga Fault are considered synthetic or Riedel (R) structures, with the same sinistral kinematics, such as the case of the Honda and La Lejía faults. The structures of the central block (Los Santos, La Mojarra, and Las Calaveras faults) are parallel to each other and the Bucaramanga Fault,

so they show similar sinistral transpressional kinematics. The southwestern block is characterized by greater geological complexity, with structures in different orientations, traces subparallel to the Los Santos Fault with reverse slip (e.g., La Chivatera Fault), and traces close to a W-E trend defined as dextral transtensional to normal faults (e.g., La Pilonera, Paso Grande and Zanjón La Vega).

Similar studies show that the degree of fracturing is correlated with changes in lithology and is influenced by the tectonic history, diagenesis, and structural variations (e.g. Monterey Formation in California by Finkbeiner et al. 1997). Besides, the current aperture of various fracture sets and the preferential pathways for groundwater flow in fractured rock aquifers may be controlled by the most recent stress field (e.g. Serra Geral aquifer in Brazil by Fernandes et al. 2016).

The kinematics of the structures is also evidenced by the calculated stress tensors, especially the general tensor, resulting from the sum of all the measured slickensides, with a SHmax of 111° (Table 2, Fig. 7). The reliability of this general tensor is based on the similarity of the six local tensors in terms of orientation, stress regime (pure strike-slip) and fault solutions (beach balls). It allows us to assume the regional character of the SHmax, as we mentioned in Methods to determine the stress tensor. The variation of the stress field, in terms of SHmax orientation is indicated with a regional W-E orientation (Velandia et al. 2020) that changes to NW-SE near the damage zone of the Bucaramanga Fault, which can have a width of 5 to 8 km (Velandia and Bermúdez 2018). In addition, these tensors from previous works also agree on the predominance of a strike-slip stress regime. In the Mesa de Los Santos, most of the measured fault-striated planes show high dips (>70°) and low pitches (Fig. 7). Consequently, the solutions of the stress tensor show that the main fault and the associated plane (beach balls - Fig. 6) are also highly inclined, which supports the stress regime and faults kinematics as strike-slip, as seen in the geological cross-section of the Mesa de Los Santos (Fig. 6).

The 111° orientation of the SHmax obtained here is consistent with the WNW-ESE compressive stress regime calculated from focal mechanisms, and the inversion of fault-striated surfaces by Cortés and Angelier (2005) in the western flank of the Eastern Cordillera. Similarly, our findings derived from slickensides inversion provide evidence that the orientation of the stress tensor aligns with the WNW-ESE SHmax observed in the majority of focal mechanisms located near the mesa (Fig. 1), meaning that it corresponds with the current stress field for the northern part of the cordillera. This deduction is also supported by García-Delgado et al. (2022) from the analysis of focal mechanisms and GPS data. At a local scale, the SHmax trajectories can undergo alterations due to the influence of the Pamplona Wedge and a regional strike-slip structure such as the Bucaramanga Fault (Velandia et al. 2020), indicating potential deflection of the stress tensor. It is worth making clear that our examinatios of the SHmax is centered on cortical earthquakes and does not encompass seismicity from the Bucaramanga Seismic Nest (± 150 km), since this seismicity does not provide insights into cortical brittle deformation, thus focal mechanisms from that depth have been excluded from our analysis.

The dilatation of fractures and their ability to transmit fluid is directly related to their aperture, which is controlled by the resolved normal stress to the plane, and depends on the magnitude and direction of the principal stresses relative to the fracture (Ferrill et al. 1999). When considering all the measured fractures from the Mesa de Los Santos their high dip angles are particularly notable (Fig. 5, pole density diagrams). The vertical connection of aquifers could be associated with the sub-vertical tectonic fracture zones generated by strike-slip regimes, which then connect with horizontal transmissive fractures at specific depths, as well as along the subhorizontal bedding of the mesa landform.

Despite the dispersion of the planes in the northern block, a variation of up to 60° for the main populations (azimuth from 80° to 140°) is noted, which can be considered as shear or conjugate fractures, with the bisector (azimuth of 110°) corresponding to the SHmax. In the central block, the fractures are mainly oriented in one direction, with a range varying from 100° to 130° in azimuth, which could be averaged at 115° and assumed as the direction of the SHmax if they are the tension fractures (Mode I). This direct tensor analysis is not possible in the southwestern block given the dispersion of the planes, which reflect the orientation of the different geological faults in the block (S-N, WNW-ESE, and ENE-WSW), although one of the trends may be related to the orientation of the SHmax (WNW-ESE). It is interesting that an analysis of fault orientation in the area (performed with FracPaQ, by Tarazona-Lizcano et al. 2021), including

the central and southwestern blocks, shows a general WNW-EWE trend with an average azimuth of 110°. This is in good agreement with the SHmax orientation calculated in the present study, which corroborates an opening nature of the faults within this trend.

The SHmax of 111° confirms the sinistral kinematics of the NW-SE faults, located closer to the Bucaramanga Fault, as well as the subparallel faults of the central block (Figs. 5 and 7). Regarding the apparent dextral motion of the Potreros and El Aljibe faults, the evidence is less clear. On one hand, these faults run parallel to the main tensor (SHmax), and therefore may better be assumed to be normal faults. On the other hand, this is contradicted by the planes measured for the El Aljibe Fault with similar orientation (S62), which indicate sinistral kinematics (Fig. 6). In a more regional view, two parallel faults (Potreros and El Aljibe) show minor dextral faults between them and connecting at low angles, so that, it is possible to interpret a duplex structure by dextral strike-slip kinematics. However, the SHmax of 111° implies a transpressional regime for the S-N faults, with a preponderant reverse component, as well as a transtensional regime and dextral slip for the faults with W-E orientation (e.g. those located in the southwestern block) and dextral kinematics for the Los Montes and San Javier faults (ENE strike) located to the north (Figs. 5 and 6). The comprehensive findings significantly enhance prior observations regarding a strike-slip stress regime toward the north of the Los Santos Fault and a compressive regime to the south of the fault (Velandia 2010).

5.2 Fracture patterns and potential flow directions

The anisotropic permeability in fractured aquifers is influenced by the abundance and distribution of faults, fractures, and the permeability directly associated to the damage zones (Ferrill et al. 1999). Faults and fractures that are oriented perpendicular to the maximum principal stress tend to close, resulting in reduced permeability. Conversely, the permeability perpendicular to the direction of the minimum principal compressive stress is greater, as fractures likely have a larger aperture (Carlsson and Olsson 1979). For the Mesa de Los Santos, the quantitative analysis of joint orientations and fracture patterns, performed with FracPaQ indicates that the main fracture trends (NW-SE) and flow directions coincide

more clearly. Furthermore, it is possible to deduce that the orthogonal fracture families (tension or Mode I) are related to the most recent and shallow deformation of the crust and that the general tensor at 111° azimuth is also evidenced by the number of fractures showing similar orientations, as found by Tarazona-Lizcano et al. (2021) for the southern mapped structures.

It is possible for water to flow from the zone of greater precipitation (NE of the Mesa de Los Santos – Fig. 2) towards the south. However, it should be noted that flow through fractures exhibiting NE-SW trends is also a possibility. In an anisotropic stress field, certain faults will be more favorably oriented for slip while others for locking, even if the distribution of fault and fracture orientations is isotropic. This characteristic enhances transmissivity in the direction of maximum horizontal stress, resulting in transmissivity anisotropy (Ferrill et al. 1999). Faults that have favorable orientations for slip or dilation serve as potential flow pathways. It is important to note that the processes altering the permeability of large faults and fracture systems also apply to smaller-scale fractures and faults (Ferrill et al. 1999; Sweetkind and Williams-Stroud 1996). Furthermore, we are aware that the bedding planes are an additional factor for the water flow estimation, meaning that the SW strata tilting (Fig. 3) favors NE-SW and N-S flow.

The extrapolation of intensity, density, and line connectivity data, obtained by FracPaQ to the surface facilitated the creation of maps (Figs. 8 and 10). These maps illustrate that the highest values of each parameter are concentrated to the south of the Mesa de Los Santos, particularly in the central block, within the sandstones of the upper member of the Los Santos Formation. This observation corroborates the findings of Tarazona-Lizcano et al. (2021) who reported similar intensity and density values in sites near La Mojarra Fault. The connectivity within a fractured rock aquifer, although closely related to fracture properties such as fracture density, orientation, length, and aperture, is an independent factor that significantly impacts the hydraulic behavior of the fracture network. It is important to note that even in densely fractured rock masses, the connectivity and permeability may remain low if the fractures have a similar orientation with limited intersections (Mortimer et al. 2011). Additionally, certain highly transmissive fracture zones may lack connectivity within the overall network, exhibiting a strong scale dependency on the collected data (Shapiro et al. 2007). The connectivity of a

fractured rock aquifer is influenced by various factors including the spatial distribution of fracture densities (fractures per unit volume), orientations (strike and dip), planar dimensions (area or trace extent), and hydraulic apertures (National Research Council 1996).

The results appear to be "discouraging" when compared with the annual precipitation map (Fig. 2), which indicates the highest values towards the NE of the mesa. This finding aligns with the conclusions of Becerra and Parra (2016) who observed a higher average multiannual precipitation value in the northern sector of the Mesa de Los Santos compared to the southern sector. This precipitation pattern is consistent with our analyzed data from 2000 to 2020. Furthermore, these authors suggest that the upper member of the Los Santos Formation is the sequence that mainly assumes the water catchment. Assuming that the same quartz sandstones (upper member of the Los Santos Formation), are present in the northern sector, the higher humidity in that region may have led to a greater weathering and disturbance of the fracture planes (homogenization), resulting in lower intensity and density values in the FracPaQ analysis, and subsequently affecting connectivity. It is important to note that secondary processes such as weathering (Fernandes et al. 2016), uplift, unloading, and fracture deformation in response to the in-situ stress field (Mortimer et al. 2011) can modify the permeability and connectivity of a fracture network. However, the same weathering factor may increase the porosity of the sandstone strata.

These outcomes are partially coincident with the fracture density presented by Contreras (2008), Díaz et al. (2009); Pinto et al. (2007) and Tarazona-Lizcano et al. (2021), showing low values in the southwestern block and the flatter and higher parts of the northern block, and highlighting the role of fractures in the hydrogeology of the Mesa de Los Santos. Here we document the importance of the alignment between the NW-SE strike-slip faults and the stress tensor (SHmax of 111°), emphasizing that these structures have a transtensional nature. The more parallel to the stress tensor, the more normal and open they generally will be, though Becerra and Parra (2016) establish an E-W groundwater direction flow for the northern sector of the Mesa de Los Santos. Our findings suggest that the recharge occurs from the NE of the mesa to the south or SE, taking advantage of the general dip direction of the sandstones (average DipDir/Dip of 220°/10°), and being redirected through the NW-SE

fractures (open) to eventually recharge the potential aquifers of the lower member of the Los Santos Fm. and the sandy levels at the top of the Rosa Blanca Fm. (Fig. 3).

Equally important is to consider the cortical seismicity and that the Mesa de Los Santos is the epicentral zone for the Bucaramanga Seismic Nest (we show the location of earthquakes with Magnitud > 5, Fig. 1). The consistent seismic activity in this region could potentially alter fracture interconnections, exerting either a positive or negative influence on the potential groundwater flow. Water levels within well-aquifer systems are susceptible to fluctuation due to earthquakes, as seismic waves can impact them in diverse ways, including their influence on fluid pressure (Roeloffs et al. 2003). The most significant fluctuations in water levels stem from the passage of surface waves, particularly Rayleigh waves generated by distant seismic events (Liu et al. 1989; Matsumoto 1992; Roeloffs 1998). Typically, these variations correlate with the magnitude of the earthquakes and might exhibit an inverse relationship with hypocentral distance (Roeloffs et al. 2003). Nonetheless, studies examining water level changes associated with seismic activity specifically in Mesa de Los Santos have not been undertaken, highlighting a potential area for future research.

6 Conclusion

The Mesa de Los Santos consists of three distinct blocks or zones: the northern, central, and southwestern. Each block exhibits unique internal structures with characteristic orientations, and the major boundaries between them are defined by the Potreros and Los Santos faults. A comprehensive analysis of approximately 1800 fracture planes measured in the area reveals a predominance of high inclination (>70°) fractures, with conjugate families observed in the northern block and tension (Mode I) observed in the central block. The interaction between the major faults (NW-SE) and the minor transverse faults reveals the presence of a strike-slip duplex zone located southward of the northern block, between El Aljibe and Potreros faults.

The stress tensors were determined using data obtained from six field stations where striated planes were available. The analysis revealed a prevailing stress tensor orientation of WNW-ESE, involving

newly formed and reactivated faults, which is attributed to the current stress field in the area, characterized by a strike-slip regime. This stress tensor coincides with the bisector calculated for the conjugate fractures of the northern block and the Mode I fractures observed in the central block. Considering the structural homogeneity of the mesa, we calculated a general stress tensor with a SHmax of 111° (from 126 striated planes) that governs the deformation in the Mesa de Los Santos.

Fracture pattern quantification was conducted using FracPaQ at 62 field stations. The intensity and density data of the discontinuity planes were interpolated using the Kriging method to generate maps. These maps generally indicate the highest values in the central block, where weathering of the sandstones of the upper member of the Los Santos Fm. is less pronounced, and lower values in the northern part of the Mesa de Los Santos, despite experiencing higher precipitation and aquifer recharge. When assessing fluid transit possibilities, the best connectivity values are found in the southern region of the mesa, where precipitation is comparatively lower. However, the presence of open NW-SE fractures and faults, combined with the gentle southwest dip of the strata, suggest the potential flow from the northern part of the mesa.

Acknowledgments

Author Contribution

All authors contributed to the study conception and design.

Material preparation and data collection: Sergio GARCÍA-ARIAS, Yessenia TARAZONA, María Camila VARGAS and Francisco VELANDIA; Investigation and Writing - original draft preparation: Sergio GARCÍA-ARIAS and Francisco VELANDIA; Writing - review and editing: Francisco VELANDIA, Angélica ALVAREZ, Sergio GARCÍA-ARIAS and José D. SANABRIA-GÓMEZ; Supervision: Francisco VELANDIA and José D. SANABRIA-GÓMEZ

All authors read and approved the final manuscript.

Ethics Declaration

Availability of Data/Materials: The datasets generated during this study are available from the corresponding author upon reasonable request and within the framework of cooperation agreements and scientific research projects.

Conflict of Interest: The authors declare no conflict of interest.

References

Alarcón CM, Clavijo-Torres J, Mantilla-Figueroa LC, et al. (2020) A new proposal on ages of the sedimentary record of Bocas and Jordan formations and their relationship with the development of the magmatic activity of the Santander Plutonic Group (Eastern Cordillera, Colombia). Rev Acad Col Cienc Exact Fís Nat 44 (173): 1137-1151. https://doi.org/10.18257/raccefyn.1208 (In Spanish)

Alarcón CM, Rodríguez JG (2019) Stratigraphy, facies, and paleoenvironment of sedimentation of the Jordan Formation: a fluvio-lacustrine register with incidence of volcanic activity. Undergraduate thesis, Universidad Industrial de Santander. (In Spanish) https://noesis.uis.edu.co/handle/20.500.14071/13047

Allmendinger RW, Cardozo N, Fisher DM (2011) Structural Geology Algorithms. Cambridge University Press. https://doi.org/10.1017/CBO9780511920202

Angelier P (1994) Fault slip analysis and palaeostress reconstruction. In Continental Deformation. Oxford: Pergamon Press. pp 53-100.

Barton CA, Zoback MD, Moos D (1995) Fluid flow along potentially active faults in crystalline rock. Geology 23(8): 683-686. https://doi.org/10.1130/0091-7613(1995)023<0683:FFAPAF>2.3.CO;2

Becerra NJ, Parra CG (2016) Water balance to estimate potential recharge in Mesa de Los Santos and groundwater flow direction. Undergraduate thesis, Universidad Industrial de Santander. (In Spanish)

Bredehoeft JD (1997) Fault permeability near Yucca Mountain. Water Res Research 33 (11): 2459-2463. https://doi.org/10.1029/97WR01710

Cardozo N, Allmendinger RW (2013) Spherical projections with OSXStereonet. Computers and Geosciences 51: 193-205. https://doi.org/10.1016/j.cageo.2012.07.021

Carlsson A, Olsson T (1979) Hydraulic conductivity and its stress dependence. In: Organization for Economic Co-operation and Development (eds.), Workshop on Low-Flow, Low-Permeability Measurements in Largely Impermeable Rocks. Paris, France. pp 249-259.

Cediel F (1698) The Girón group, a Mesozoic molasses from the Eastern Cordillera. Bol Geológico 16(1-3): 5-96. https://revistas.sgc.gov.co/index.php/boletingeo/article/view/108 (In Spanish)

Contreras NM (2008) Analysis of the Fracture Present in the Los

Santos Formation to the North and Center of the Mesa de Los Santos, Department of Santander. Undergraduate thesis, Universidad Industrial de Santander. (In Spanish)

Cortés M, Angelier J (2005) Current states of stress in the northern Andes as indicated by focal mechanisms of earthquakes. Tectonophysics 403: 29-58.

Davis G H, Reynolds SJ, Kluth CF (2011) Structural geology of rocks and regions (3rd ed.). John Wiley and Sons, Inc.

Delvaux D (2001) Win-Tensor (5.9.0). http://damiendelvaux.be/Tensor/WinTensor/win-tensor.html

Delvaux D, Moeys R, Stapel G, et al. (1997) Paleostress reconstructions and geodynamics of the Baikal region, Central Asia, Part 2. Cenozoic rifting. Tectonophysics 282(1-4): 1-38. https://doi.org/10.1016/S0040-1951(97)00210-2

Delvaux D, Sperner B (2003) New aspects of tectonic stress inversion with reference to the TENSOR program. Geological Society, London, Special Publications 212(1): 75-100. https://doi.org/10.1144/GSL.SP.2003.212.01.06

Díaz EJ, Contreras NM, Pinto JE, et al. (2009) Preliminary hydrogeological evaluation from geological formations of Mesa de Los Santos, Santander. Bol Geol 31. https://revistas.uis.edu.co/index.php/revistaboletindegeologia/article/view/167 (In Spanish)

Doblas M (1998) Slickenside kinematic indicators. Tectonophysics 295(1-2): 187-197. https://doi.org/10.1016/S0040-1951(98)00120-6

Fernandes AJ, Maldaner CH, Negri F, et al. (2016) Aspects of a conceptual groundwater flow model of the Serra Geral basalt aquifer (Sao Paulo, Brazil) from physical and structural geology data. Hydrogeol J 24 (5): 1199-1212. https://doi.org/10.1007/s10040-016-1370-6

Ferrill DA, Winterle J, Wittmeyer G, et al. (1999) Stressed rock strains groundwater at Yucca Mountain, Nevada. GSA Today (A Publication of the Geological Society of America) 9: 1-8.

Finkbeiner T, Barton CA, Zoback MD (1997) Relationships among in-situ stress, fractures and faults, and fluid flow: Monterey Formation, Santa Maria Basin, California. AAPG Bulletin 81. https://doi.org/10.1306/3B05C6FE-172A-11D7-8645000102C1865D

Fossen H (2010) Structural Geology. Cambridge University Press. https://doi.org/10.1017/CBO9780511777806

Fridrich CJ, Dudley WW, Stuckless JS (1994) Hydrogeologic analysis of the saturated-zone ground-water system, under Yucca Mountain, Nevada. J Hydrol 154 (1-4): 133-168. https://doi.org/10.1016/0022-1694(94)90215-1

Frohlich C (1992) Triangle diagrams: ternary graphs to display similarity and diversity of earthquake focal mechanisms. Phys Earth Planet Inter 75 (1-3): 193-198. https://doi.org/10.1016/0031-9201(92)90130-N

Frohlich C (2001) Display and quantitative assessment of distributions of earthquake focal mechanisms. Geophys J Int 144 (2): 300-308. https://doi.org/10.1046/j.1365-246x.2001.00341.x

García-Delgado H, Machuca S, Velandia F, et al. (2020) Along-strike variations in recent tectonic activity in the Santander Massif: New insights on landscape evolution in the Northern Andes. J South Am Earth Sci 98: 102472. https://doi.org/10.1016/j.jsames.2019.102472

García-Delgado H, Velandia F, Bermúdez MA, et al. (2022) The present-day tectonic regimes of the Colombian Andes and the role of slab geometry in intraplate seismicity. Int J Earth Sci 111: 2081-2099. Springer Science and Business Media LLC. https://doi.org/10.1007/s00531-022-02227-9

Healy D, Rizzo R (2019) FracPaQ: Fracture pattern quantification. (User guide version 2.6). https://github.com/DaveHealy-github/FracPaQ

Healy D, Rizzo RE, Cornwell DG, et al. (2017) FracPaQ: A MATLAB™ toolbox for the quantification of fracture patterns. J Struct Geol 95: 1-16. https://doi.org/10.1016/j.jsg.2016.12.003

Huang Q, Angelier J (1989) Inversion of field data in fault tectonics to obtain the regional stress-II. Using conjugate fault sets within heterogeneous families for computing palaeostress axes. Geophys J Int 96 (1): 139-149. https://doi.org/10.1111/j.1365-246X.1989.tb05256.x

IDEAM (2022) Instituto de Hidrología, Meteorología y Estudios Ambientales IDEAM. http://www.ideam.gov.co (Accessed on 1 July 2022)

Isaacs CM (1984) Geology and Physical Properties of the Monterey Formation, California. Annual California Regional Meeting: Society of Petroleum Engineers. https://doi.org/10.2118/12733-MS

Julivert M (1958) The Morphostructure of the Mesas Zone at SW of Bucaramanga (Colombia S. A.). Bol Geol 1: 7-43. https://revistas.uis.edu.co/index.php/revistaboletindegeologia/article/view/3994 (In Spanish)

Julivert M, Barrero D, Navas GJ (1964) Geología de la Mesa de Los Santos. Bol Geol 18: 5-11. https://doi.org/10.18273/revbol

Kellogg JN, Vega V, Stailings TC, et al. (1995) Tectonic development of Panama, Costa Rica, and the Colombian Andes: Constraints from Global Positioning System geodetic studies and gravity. pp 75-90. https://doi.org/10.1130/SPE295-p75

Laverde F (1985) The Los Santos Formation: a continental deposit prior to the marine ingress of the Cretaceous, Cretaceous Project, Chapter XX. Publ Geol Espec INGEOMINAS 16: 1-24. (In Spanish)

Laverde F (2023) Revisiting the latest Jurassic-earliest Cretaceous Los Santos Formation, Eastern Cordillera of Colombia. A - The history of its origin and the lowermost part of the unit. Bol Geológico 50 (1). https://doi.org/10.32685/0120-1425/bol.geol.50.1.2023.689

Liu LB, Roeloffs E, Zheng XY (1989) Seismically induced water level fluctuations in the Wali Well, Beijing, China. J Geophys Res 94 (B7): 9453. https://doi.org/10.1029/jb094ib07p09453

Londoño JM, Quintero S, Vallejo K, et al. (2019) Seismicity of Valle Medio del Magdalena basin, Colombia. J South Am Earth Sci 92: 565-585. https://doi.org/10.1016/j.jsames.2019.04.003

Long JCS, Karasaki K, Davey A, et al. (1991) An inverse approach to the construction of fracture hydrology models conditioned by geophysical data. Int J Rock Mech Min Sci Geomech Abstr 28 (2-3): 121-142. https://doi.org/10.1016/0148-9062(91)92162-R

Machuca S, García-Delgado H, Velandia F (2021) Studying active fault-related folding on tectonically inverted orogens: A case study at the Yariguíes Range in the Colombian Northern Andes. Geomorphology 375: 107515. https://doi.org/10.1016/j.geomorph.2020.107515

Malavé G, Suárez G (1995) Intermediate-depth seismicity in northern Colombia and western Venezuela and its relationship to Caribbean plate subduction. Tectonics 14 (3): 617-628. https://doi.org/10.1029/95TC00334

Mantilla-Figueroa L, García Ramírez C, Valencia V (2016) A Proposal to Split-Off the So-Called 'Silgará Formation' (Santander Massif, Colombia) Supported On Detrital U-Pb Zircon Ages. Bol Geol 38 (1): 33-50. https://doi.org/10.18273/revbol.v38n1-2016002 (In Spanish)

Manzocchi T (2002) The connectivity of two-dimensional networks of spatially correlated fractures. Water Resour Res 38 (9): 1-1-1-20. https://doi.org/10.1029/2000WR000180

Marrett R, Peacock DCP (1999) Strain and stress. J Struct Geol 21 (8-9): 1057-1063. https://doi.org/10.1016/S0191-8141(99)00020-6

Matsumoto N (1992) Regression analysis for anomalous changes of ground water level due to earthquakes. Geophys Res Lett 19 (12): 1193-1196. https://doi.org/10.1029/92gl01042

Mauldon M, Dunne WM, Rohrbaugh MB (2001) Circular scanlines and circular windows: new tools for characterizing the geometry of fracture traces. J Struct Geol 23 (2-3): 247-258. https://doi.org/10.1016/S0191-8141(00)00094-8

Mortimer L, Aydin A, Simmons CT, et al. (2011) The role of in situ stress in determining hydraulic connectivity in a fractured rock aquifer (Australia). Hydrogeol J 19 (7): 1293-1312. https://doi.org/10.1007/s10040-011-0760-z

NASA (2020) Alaska Satellite Facility. https://vertex.daac.asf.alaska.edu/ (Accessed on 1 July 2020)

National Research Council (1996) Rock Fractures and Fluid Flow:

contemporary understanding and applications. National Academies Press.
https://doi.org/10.17226/2309

Oda M (1982) Fabric Tensor for Discontinuous Geological Materials. Soils Found 22 (4): 96-108.
https://doi.org/10.3208/sandf1972.22.4_96

Oda M, Hatsuyama Y, Ohnishi Y (1987) Numerical experiments on permeability tensor and its application to jointed granite at Stripa Mine, Sweden. J Geophys Res 92 (B8): 8037.
https://doi.org/10.1029/JB092iB08p08037

Paris G, Machette MN, Dart RL, et al. (2000) Map and database of Quaternary faults and folds in Colombia and its offshore regions. US Geological Survey.
https://doi.org/10.3133/ofr00284

Petit JP (1987) Criteria for the sense of movement on fault surfaces in brittle rocks. J Struct Geol 9 (5-6): 597-608.
https://doi.org/10.1016/0191-8141(87)90145-3

Pinto JE, Clavijo J, Gómez S, et al. (2007) Geological and hydrogeological research project in Mesa de Los Santos, northeast sector of Curití and western edge of the Santander Massif, department of Santander. (Explanatory report on the geological and hydrogeological research in Mesa de Los Santos and the Northeast sector of Curití). Instituto Colombiano de Geología y Minería. Bucaramanga, Colombia. (In Spanish)

Planet Team (2018) Planet application program interface: In space for life on earth. https://api.planet.com

Prieto GA, Beroza GC, Barrett SA, et al. (2012) Earthquake nests as natural laboratories for the study of intermediate-depth earthquake mechanics. Tectonophysics 570-571: 42-56.
https://doi.org/10.1016/j.tecto.2012.07.019

Roeloffs EA (1998) Persistent water level changes in a well near Parkfield, California, due to local and distant earthquakes. J Geophys Res Solid Earth 103 (B1): 869-889.
https://doi.org/10.1029/97jb02335

Roeloffs E, Sneed M, Galloway DL, et al. (2003) Water-level changes induced by local and distant earthquakes at Long Valley caldera, California. J Volcanol Geotherm Res 127 (3-4): 269-303.
https://doi.org/10.1016/s0377-0273(03)00173-2

Rohrbaugh MB, Dunne WM, Mauldon M (2002). Estimating Fracture Trace Intensity, Density, and Mean Length Using Circular Scan Lines and Windows. AAPG Bulletin 86 (12): 2089−2104. https://doi.org/10.1306/61EEDE0E-173E-11D7-8645000102C1865D

Royero JM, Clavijo J (2001) Generalized Geological Map department of Santander. Instituto Colombiano de Geología y Mineria. Bogotá, Colombia. (In Spanish)

Sanderson DJ, Nixon CW (2015) The use of topology in fracture network characterization. J Struct Geol 72: 55-66.
https://doi.org/10.1016/j.jsg.2015.01.005

Sassi W, Faure J-L (1996) Role of faults and layer interfaces on the spatial variation of stress regimes in basins: inferences from numerical modelling. Tectonophysics 266 (1-4): 101-119.
https://doi.org/10.1016/S0040-1951(96)00185-0

Shapiro AM, Hsieh PA, Burton WC, et al. (2007) Integrated multi-scale characterization of ground-water flow and chemical transport in fractured crystalline rock at the Mirror Lake Site, New Hampshire. pp 201-225.
https://doi.org/10.1029/171GM15

Shapiro AM, Ladderud JA, Yager RM (2015) Interpretation of hydraulic conductivity in a fractured-rock aquifer over increasingly larger length dimensions. Hydrogeol J 23 (7): 1319-1339.
https://doi.org/10.1007/s10040-015-1285-7

Suzuki K, Oda M, Yamazaki M, et al. (1998) Permeability changes in granite with crack growth during immersion in hot water. Int J Rock Mechan Min Sci 35 (7): 907-921.

https://doi.org/10.1016/S0148-9062(98)00016-3

Sweetkind DS, Williams-Stroud SC (1996) Characteristics of fractures at Yucca Mountain. Nevada, Synthesis Report: US Geological Survey Administrative Report.

Taboada A, Rivera L, Fuenzalida A, et al. (2000) Geodynamics of the northern Andes: subductions and intracontinental deformation (Colombia). Tectonics 19 (5): 787-813.

Tarazona-Lizcano Y, Vargas-López MC, Velandia F (2021) Quantitative analysis of the fracture systems and groundwater implications in the south zone of the Mesa de Los Santos, Santander - Colombia. Bol Geol 43 (3). (In Spanish)
https://doi.org/10.18273/revbol.v43n3-2021005

The MathWorks Inc (2022) MATLAB version: 9.13.0 (R2022b). The MathWorks Inc. https://www.mathworks.com

Tripathy V, Saha D (2013) Plate margin paleostress variations and intracontinental deformations in the evolution of the Cuddapah basin through Proterozoic. Precambrian Res 235: 107-130.
https://doi.org/10.1016/j.precamres.2013.06.005

Van der Hilst R, Mann P (1994) Tectonic implications of tomographic images of subducted lithosphere beneath northwestern South America. Geology 22 (5): 451-454.
https://doi.org/10.1130/0091-7613(1994)022<0451:TIOTIO>2.3.CO;2

Vargas CY (2008) Geological cartography at a scale of 1:25.000 of the Mesa de Los Santos, department of Santander. Undergraduate thesis, Universidad Industrial de Santander. (In Spanish)

Velandia F (2010) Analysis of fractures for groundwater exploration in the center of Santander. In: Hidrogeología para la gestión del recurso hídrico, Universidad de Antioquia. pp 149-158. (In Spanish)

Velandia F (2017) Kinematics of the major faults of the Santander Massif - emphasis on the structural model and temporality to the south of the Bucaramanga Fault. PhD tesis, Universidad Nacional de Colombia. p 209. (In Spanish)

Velandia F, Bermúdez MA (2018) The transpressive southern termination of the Bucaramanga fault (Colombia): Insights from geological mapping, stress tensors, and fractal analysis. J Struct Geol 115: 190-207.
https://doi.org/10.1016/j.jsg.2018.07.020

Velandia F, Silva G, Morales C, et al. (2007) Kinematic analysis of the central region of the Department of Santander. XI Congreso Colombiano de Geología. (In Spanish)

Velandia F, García-Delgado H, Zuluaga CA, et al. (2020) Present-day structural frame of the Santander Massif and Pamplona Wedge: The interaction of the Northern Andes. J Struct Geol 137: 104087.
https://doi.org/10.1016/j.jsg.2020.104087

Ward D, Goldsmith R, Jimeno A, et al. (1977) Geological map of the quadrangle H-12 Bucaramanga. Scale 1:100.000. Instituto Colombiano de Geología y Minería. Colombia. (In Spanish)

Yong Technology Inc (2014) GeoRose.
http://www.yongtechnology.com/download/geoRose
(Accessed on 1 July 2022)

Zarifi Z, Havskov J (2003) Characteristics of Dense Nests of Deep and Intermediate-Depth Seismicity. Adv Geophys 46 (C): 237-278.
https://doi.org/10.1016/S0065-2687(03)46004-4

Zeeb C, Gomez-Rivas E, Bons P, et al. (2013). Evaluation of sampling methods for fracture network characterization using outcrops. AAPG Bulletin 97 (9): 1545−1566.
https://doi.org/10.1306/02131312042

Zoback ML (1992) First- and second-order patterns of stress in the lithosphere: The World Stress Map Project. J Geophys Res 97 (B8): 11703.
https://doi.org/10.1029/92JB00132